Competing effects of rare gas atoms in matrix isolation spectroscopy: A case study of vibrational shift of BeO in Xe and Ar matrices

Akira Nakayama, Keisuke Niimi, Yuriko Ono, and Tetsuya Taketsugu

Citation: J. Chem. Phys. **136**, 054506 (2012); doi: 10.1063/1.3680562
View online: http://dx.doi.org/10.1063/1.3680562
View Table of Contents: http://jcp.aip.org/resource/1/JCPSA6/v136/i5
Published by the American Institute of Physics.

Competing effects of rare gas atoms in matrix isolation spectroscopy: A case study of vibrational shift of BeO in Xe and Ar matrices

Akira Nakayama,[a] Keisuke Niimi, Yuriko Ono, and Tetsuya Taketsugu
Division of Chemistry, Graduate School of Science, Hokkaido University, Sapporo 060-0810, Japan

(Received 3 December 2011; accepted 11 January 2012; published online 3 February 2012)

We investigate the vibrational shift of beryllium oxide (BeO) in Xe matrix as well as in Ar matrix environments by mixed quantum-classical simulation and examine the origin of spectral shift in details. BeO is known to form strong chemical complex with single rare gas atom, and it is predicted from the gas phase calculations that vibrational frequencies are *blueshifted* by 78 cm^{-1} and 80 cm^{-1} upon formation of XeBeO and ArBeO, respectively. When the effects of other surrounding rare gas atoms are included by Monte Carlo simulations, it is found that the vibrational frequencies are *redshifted* by 21 cm^{-1} and 8 cm^{-1} from the isolated XeBeO and ArBeO complexes, respectively. The vibrational shift of XeBeO in Ar matrix is also calculated and compared with experimental data. In all simulations examined in this paper, the calculated vibrational frequency shifts from the isolated BeO molecule are in reasonable agreement with experimental values. The spectral shift due to the rare-gas-complex formation of RgBeO (Rg = Xe or Ar) is not negligible as seen in the previous studies, but it is shown in this paper that the effects of other surrounding rare gas atoms should be carefully taken into account for quantitative description of the spectral shifts and that these two effects are competing in vibrational spectroscopy of BeO in matrix environments. © *2012 American Institute of Physics*. [doi:10.1063/1.3680562]

I. INTRODUCTION

Matrix isolation spectroscopy is a powerful tool to measure various properties of chemical species by isolating them in an ideal condition for spectroscopic measurements, and therefore sometimes it allows us to obtain valuable information even on unstable molecules.[1] Since these spectra are usually obtained at very low temperatures, they are almost free from perturbations due to thermal fluctuations, thus enabling one to perform highly precise measurements. Rare gas atoms are almost exclusively used as a matrix medium, and since they are chemically inert, it is naturally assumed that the effect of surrounding rare gas atoms is marginal and in fact spectral shifts due to the presence of rare gas atoms are typically less than 0.5%.

However, there have been several studies which reported that the rare gas atoms can form chemical complexes with some molecules,[2–4] and in some cases their interactions are strong enough that they are regarded as more like chemical compounds. In these situations, non-negligible spectral shifts are observed upon formation of rare gas complexes, and it is necessary to take into account this shifts when analyzing the spectroscopic data if obtained in matrix environments.

Beryllium oxide (BeO) has long been studied in this context since it is known to form chemical complexes with rare gas atoms (Rg = Ar, Kr, Xe).[5] When the RgBeO complex is formed, the blueshift in vibrational spectrum is observed.[6] Veldkamp and Frenking performed *ab initio* calculations on these complexes and found that charge-induced dipole interaction is the source of these complex formation.[7] They reproduced the vibrational shift to higher wave number observed in the experiments. In their calculations, the shifts upon formation of XeBeO and ArBeO were estimated to be 110 cm^{-1} and 122 cm^{-1}, respectively. However, the shift in XeBeO (ArBeO) complex is larger than that observed in the Xe (Ar) matrix experiments,[8] which was about 34 (62) cm^{-1}, and it is anticipated that the effect of surrounding media may not be negligible. At the best of our knowledge, there is no report which investigates the effects of surrounding rare gas atoms on vibrational shifts for these complexes quantitatively. The spectroscopic data obtained experimentally for BeO and RgBeO in various rare gas matrices are tabulated in Table I.

In this paper, we investigate the vibrational shift of BeO in Xe matrix as well as in Ar matrix environments with mixed quantum-classical simulation and examine the origin of spectral shift in details from the viewpoints of complex-formation and perturbations from surrounding atoms. In particular, we examine the vibrational shift of XeBeO in Xe and Ar matrices and ArBeO in Ar matrix, where the experimental data are available.

II. SIMULATION METHODS

In this section, we briefly describe the simulation method used to obtain the vibrational spectra of a target molecule in rare gas matrix environments. The total system is divided into quantum and classical parts, where the quantum part consists of the target molecule represented by N_q normal coordinates while the classical part is composed of N rare gas atoms. The hybrid quantum-classical Hamiltonian of the whole system is

[a]Author to whom correspondence should be addressed. Electronic mail: akira-n@sci.hokudai.ac.jp.

TABLE I. Vibrational frequency (in cm^{-1}) of Be-O stretching motion of RgBeO complexes observed in various rare gas matrices.

	BeO	ArBeO	KrBeO	XeBeO
Gas phase	1464[a]	...	...	...
In Ar matrix	...	1526[b]	1522[b]	1517[b]
In Kr matrix	...	...	1512[c]	...
In Xe matrix	...	...	...	1498[c]

[a]Reference 9.
[b]Reference 6.
[c]Reference 8.

then assumed to have the following pairwise-additive form:

$$H = \sum_{i=1}^{N_q} \frac{1}{2}\hat{p}_i^2 + \sum_{i=1}^{N} \frac{1}{2}\mathbf{P}^{(i)} + V_{\text{qm}}(\hat{\mathbf{q}}) + \sum_{i=1}^{N} V_{\text{qm-Rg}}(\hat{\mathbf{q}}, \mathbf{R}^{(i)}) + \sum_{i<j}^{N} V_{\text{Rg-Rg}}(|\mathbf{R}^{(i)} - \mathbf{R}^{(j)}|) \quad (2.1)$$

where $\hat{\mathbf{q}} = \{\hat{q}_i; i = 1, \ldots, N_q\}$ and $\hat{\mathbf{p}} = \{\hat{p}_i; i = 1, \ldots, N_q\}$ represent the normal coordinates and their conjugate momenta of the target molecule, respectively. $\mathbf{R} = \{\mathbf{R}^{(i)}; i = 1, \ldots, N\}$ and $\mathbf{P} = \{\mathbf{P}^{(i)}; i = 1, \ldots, N\}$ are the coordinates and momenta of rare gas atoms, respectively. Here the center-of-mass and rotational motions of the molecule are treated classically and they are not included in the above Hamiltonian. In this work, vibrational-rotational coupling is neglected. $V_{\text{qm-Rg}}$ is the interaction potential between the molecule and rare gas atoms and it is obtained from the high-level *ab initio* calculations described below. $V_{\text{Rg-Rg}}$ is an interaction potential of rare gas atoms and this part is also determined by *ab initio* calculations.

The target molecule, which is treated quantum mechanically, is first set as a BeO molecule and the validity of the above pairwise-additive form to describe the total potential is examined in the case of BeO-Xe_N complexes. The BeO-Xe interaction potential is obtained by *ab initio* calculations, which will be described below, with BeO distance fixed at an equilibrium value, and the two-dimensional contour plot of the potential energy surface for BeO-Xe is shown in Figure 1. As seen in the figure, there is a deep minimum on the Be side in collinear geometry, which has a binding energy of 19.65 kcal/mol. When we employ the following pairwise-additive form for the potential of a BeO-Xe_2 complex,

$$V_{\text{BeO-Xe}}(\mathbf{R}^{(1)}) + V_{\text{BeO-Xe}}(\mathbf{R}^{(2)}) + V_{\text{Xe-Xe}}(|\mathbf{R}^{(1)} - \mathbf{R}^{(2)}|), \quad (2.2)$$

the minimum energy structure becomes Y-shaped, where two Xe atoms are equidistant from the Be atom as shown in Figure 2, and the total interaction energy is estimated to be 29.14 kcal/mol. *Ab initio* calculation predicts the interaction energy of 20.17 kcal/mol for this Y-shaped configuration and it is far different from the energy given by (2.2). On the other hand, for the collinear configuration, which is determined by the *ab initio* method as a local minimum structure, the interaction energies are calculated to be 20.12 and 20.56 kcal/mol by the pairwise-additive form and *ab initio* method, respectively, and they agree well with each other (see also Figure 2).

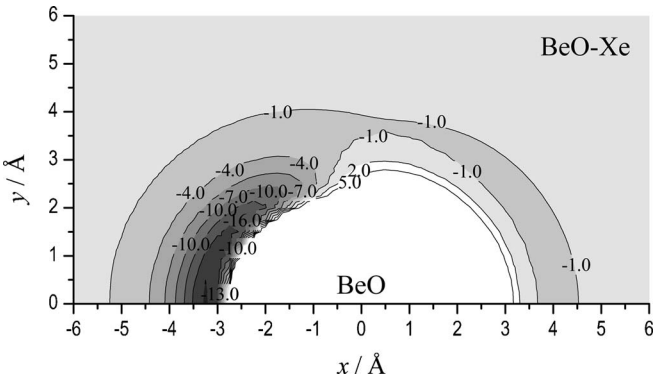

FIG. 1. Two-dimensional contour plot of the potential energy surface (in units of kcal/mol) for BeO-Xe. The internal coordinates of BeO are fixed at the equilibrium values and the origin is set to the center-of-mass of BeO. The positions of Be and O are (−0.85, 0.0) and (0.48, 0.0), respectively.

As can be apparently seen from the energies of the Y-shaped structure, potential energy defined by (2.2) is not appropriate to represent the interaction for BeO-Xe_N complexes.

From these results, it is found that the electronic structure of the Xe atom that is bound to the Be atom is strongly perturbed by the BeO molecule and a stable chemical complex XeBeO is formed, as was predicted in the previous work.[7] The electronic structure of the Xe atom in this complex would be very different from the other surrounding Xe atoms. Similar observations are seen for BeO-Ar_2, and therefore we set the XeBeO (or ArBeO) complex as a QM part in our simulation and the total potential energy term for the RgBeO-Rg_N complexes is represented as

$$V_{\text{RgBeO}}(\hat{\mathbf{q}}) + \sum_{i=1}^{N} V_{\text{RgBeO-Rg}}(\hat{\mathbf{q}}, \mathbf{R}^{(i)}) + \sum_{i<j}^{N} V_{\text{Rg-Rg}}(|\mathbf{R}^{(i)} - \mathbf{R}^{(j)}|) \quad (2.3)$$

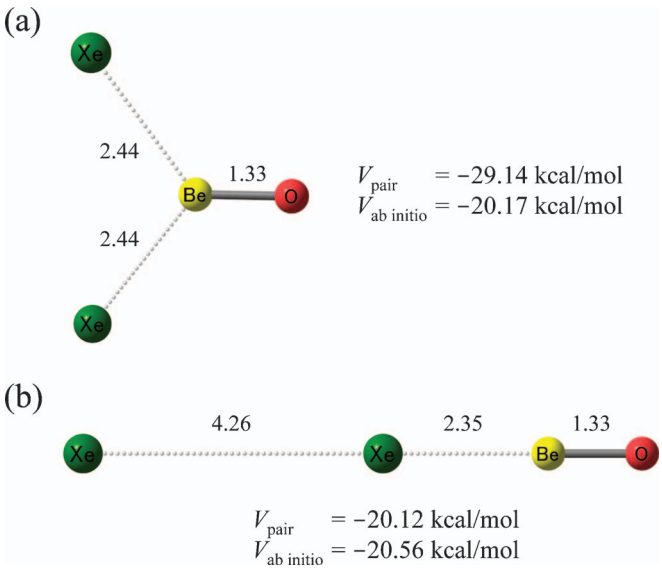

FIG. 2. Minimum energy structures of Xe_2BeO obtained by (a) the pairwise-additive model and (b) *ab initio* calculations. Bond lengths are given in unit of Å.

The validity of the above expression will be examined in Sec. III B.

A. *Ab initio* calculations

All *ab initio* potential energies are calculated by the coupled-cluster singles and doubles including the perturbative contributions of connected triple excitations [CCSD(T)] method. The excitations from Be 1*s* orbital are also included in the calculation. The cc-pCVQZ basis set is used for Be and the aug-cc-pVQZ basis sets are employed for O and Ar atoms. For Xe atoms, Stuttgart RLC ECP is employed.[10] As a preliminary calculation, the Xe-Xe potential energy curve is computed with this method. The equilibrium distance and binding energy are calculated to be $r_{\min} = 4.561$ Å and $D_e = 0.430$ kcal/mol, respectively. These values are in good agreement with those of the Lennard–Jones parameters,[11] $r_{\min} = 4.602$ Å and $D_e = 0.442$ kcal/mol, which are commonly used in simulations of solid xenon. The basis set superposition error (BSSE) corrected binding energy that is obtained by the counterpoise method becomes $D_e = 0.265$ kcal/mol and it is much smaller than that of the Lennard–Jones parameters, therefore the BSSE correction is not applied to the XeBeO-Xe interaction. For Ar-Ar interaction, the potential energy curve with the BSSE correction exhibits $r_{\min} = 3.827$ Å and $D_e = 0.238$ kcal/mol, which agree well with the reported values of Lennard–Jones parameters $r_{\min} = 3.822$ Å and $D_e = 0.238$ kcal/mol. Therefore, XeBeO-Ar and ArBeO-Ar interactions are corrected by the counterpoise method. The XeBeO-Xe, XeBeO-Ar, and ArBeO-Ar interaction potential energies are calculated for every normal coordinates of RgBeO ($\mathbf{q}$) at predetermined points represented by polar coordinates (r, θ), where r is the distance of Rg from the center-of-mass of RgBeO and θ is the angle measured from the molecular axis of RgBeO. The grid points are in the range of 2 to 8 Å and 0 to 180° with a spacing of 0.2 Å and 4.5° for r and θ, respectively. The interaction potential energies of Xe-Xe and Ar-Ar are also evaluated in the range of 3 to 20 Å and 2 to 19 Å, respectively, with a grid spacing of 0.1 Å. These energies are tabulated for use in the subsequent Monte Carlo (MC) simulations where the potential energy is evaluated by the Lagrange polynomial interpolation. All *ab initio* calculations are carried out by the MOLPRO2008.1 package.[12]

B. Potential-optimized discrete variable representation

The vibrational energy levels for the target molecule XeBeO and ArBeO are solved in the presence of surrounding Rg atoms by the discrete variable representation (DVR) method[13] using the Hamiltonian composed of the first, third, and fourth terms in the right-hand side of Eq. (2.1). Since we need to solve this equation in each configuration of Rg atoms which is sampled by the MC method, it is important to reduce the computational cost of this task. For this purpose, we employ the potential-optimized DVR (PO-DVR) method to reduce the size of the basis set.[14] The optimized one-dimensional basis set is obtained by the sinc-DVR method[15] using each normal coordinate of RgBeO with other normal coordinates set to zero. After obtaining these one-dimensional basis sets, the vibrational energy levels for the RgBeO complex in the presence of surrounding Rg atoms are solved using the basis set which is composed of direct products of each optimized one-dimensional basis set.

For RgBeO, there are three normal coordinates which correspond to Be-O stretching (q_1), Rg-Be stretching (q_2), and bending motion (q_3). In obtaining the optimized one-dimensional basis set, the sinc-DVR calculation is first performed for each normal coordinate using 200 grid points in the range of [−1.1, 1.1], [−1.9, 1.9], and [−2.0, 2.0] Å · (amu)$^{1/2}$ for q_1, q_2, and q_3, respectively. After solving the above equations, we employ the first ten eigenfunctions as an optimized one-dimensional basis set for each q_1, q_2, and q_3. This size of the basis set is large enough to obtain a converged value of fundamental frequency of Be-O stretching motion in both XeBeO and ArBeO. In the MC simulations, we use two normal modes that correspond to Be-O (q_1) and Rg-Be (q_2) stretching motions, and in this case five and three optimized one-dimensional basis functions are employed for q_1 and q_2, respectively, to save computational time. This reduced size of the basis set is still large enough to obtain a converged value when only q_1 and q_2 are used (referred to 2D-DVR below).

C. Monte Carlo simulation

The MC calculations are performed to obtain vibrational spectra of RgBeO complex in the matrix environment at finite temperatures. The sampling is performed according to the distribution $\rho(\mathbf{R}) \propto \exp(-\beta V(\mathbf{R}))$, where the potential energy is represented by

$$V(\mathbf{R}) = E^0_{\mathrm{qm}}(\mathbf{R}) + \sum_{i<j}^{N} V_{\mathrm{Rg\text{-}Rg}}(|\mathbf{R}^{(i)} - \mathbf{R}^{(j)}|). \tag{2.4}$$

In the above equation, $E^0_{\mathrm{qm}}(\mathbf{R})$ is the vibrational ground state energy in the presence of surrounding Rg atoms, which is obtained as the lowest eigenenergy in the PO-DVR equation. In the conventional MC sampling, the PO-DVR equation must be solved in each step, even if a single Rg atom that is far from the molecule is chosen to move, which gives only slight modification of the potential used for solving the PO-DVR equation.

In order to further enhance the efficiency of MC sampling, we employ the multiple Markov chain method, which is also known as the approximate potential method.[16,17] In this work, an auxiliary MC sampling is performed using the approximate potential defined by

$$V_{\mathrm{ap}}(\mathbf{R}) = \sum_{i=1}^{N} V_{\mathrm{qm\text{-}Rg}}(\hat{\mathbf{q}} = 0, \mathbf{R}^{(i)}) + \sum_{i<j}^{N} V_{\mathrm{Rg\text{-}Rg}}(|\mathbf{R}^{(i)} - \mathbf{R}^{(j)}|), \tag{2.5}$$

and after a certain number of steps on this approximate potential, the difference between the original and approximate potential is used as a criterion to restore sampling with respect to the original potential. The acceptance probability in this procedure for a trial move $\mathbf{R} \rightarrow \mathbf{R}'$ is therefore given as

$$P(\mathbf{R} \to \mathbf{R}') = \min[1, \exp\{-\beta[(V(\mathbf{R}') - V_{\rm ap}(\mathbf{R}')) - (V(\mathbf{R}) - V_{\rm ap}(\mathbf{R}))]\}]$$
$$= \min\left[1, \exp\left\{-\beta\left[\left(E^0_{\rm qm}(\mathbf{R}') - \sum_{i=1}^{N} V_{\text{qm-Rg}}(\hat{\mathbf{q}} = 0, \mathbf{R}'^{(i)})\right) - \left(E^0_{\rm qm}(\mathbf{R}) - \sum_{i=1}^{N} V_{\text{qm-Rg}}(\hat{\mathbf{q}} = 0, \mathbf{R}^{(i)})\right)\right]\right\}\right]. \quad (2.6)$$

With this method, correlation in the Markov chain on the original potential is significantly reduced. The sampling on the approximate potential is much less expensive than the original potential, since one does not need to solve the PO-DVR equation. In fact, when the number of sampling on the approximate potential is $N_s = 100$, we obtained around 95% acceptance probability in the trial move defined in Eq. (2.6). We do not investigate the systematic comparison regarding the efficiency in this paper, but from our experience significant computational saving has been achieved.

The vibrational spectra are obtained by the following simple form as

$$I(\omega) = \int d\mathbf{R}\delta(E^1_{\rm qm}(\mathbf{R}) - E^0_{\rm qm}(\mathbf{R}) - \omega)\rho(\mathbf{R}), \quad (2.7)$$

where $E^1_{\rm qm}(\mathbf{R})$ is the first vibrational excited-state energy of Be-O stretching motion in RgBeO complex.

III. RESULTS AND DISCUSSION

A. *Ab initio* calculations for BeO, XeBeO, and ArBeO

The potential energy surfaces of BeO, XeBeO, and ArBeO were computed by the CCSD(T) method, and the geometry optimization and vibrational frequency calculations were also performed. Table II summarizes equilibrium bond lengths, harmonic and fundamental frequencies of Be-O stretching motion in BeO, XeBeO, and ArBeO. The binding energy of Xe to BeO was calculated to be 19.65 kcal/mol and it is much stronger than that of the Xe-Xe interaction (0.433 kcal/mol) by two orders of magnitude. The binding energy of Ar to BeO is found to be 11.67 kcal/mol, and it is also quite strong compared to the Ar-Ar interaction (0.238 kcal/mol). The vibrational energy levels were calculated using potential-optimized basis sets, and 1D-DVR represents the calculation using a basis set only for q_1 (Be-O stretching). The results denoted by 2D-DVR were obtained using basis sets for both q_1 and q_2 (Xe-Be or Ar-Be stretching), while 3D-DVR indicates that all three basis sets were employed.

TABLE II. Equilibrium bond lengths (in Å), harmonic and fundamental frequencies (in cm^{-1}) of Be-O stretching motion for BeO, XeBeO, and ArBeO.

	r_e(Be-O)	r_e(Rg-Be)	Harmonic	Fundamental		
				1D-DVR	2D-DVR	3D-DVR
BeO	1.333	...	1483	1459	...	...
XeBeO	1.333	2.350	1558	1543	1537	1535
ArBeO	1.331	2.068	1560	1545	1539	1536
BeO (expt.)[a]	1.331	...	1487[a]		1464[b]	

[a]Reference 9.
[b]Fundamental frequency.

The fundamental frequency for BeO molecule was calculated to be 1459 cm^{-1} and is in good agreement with experimental data of 1464 cm^{-1}.[9] Upon formation of the XeBeO complex, the equilibrium bond length of r_e(Be-O) remains almost unchanged. However, spectral shifts of Be-O stretching motion by 75 cm^{-1} for harmonic frequency and 78 cm^{-1} for fundamental frequency in 2D-DVR calculation are observed. This blueshift can be attributed to the increased charge separation that is caused by the strong charge-induced dipole interaction, as was found in Ref. 7. As was pointed out previously, the frequency shift of 78 cm^{-1} is larger than that of 34 cm^{-1} measured experimentally in Xe matrix. The fundamental frequency obtained by 3D-DVR was calculated to be 1535 cm^{-1}, and the difference between the 2D-DVR and 3D-DVR methods is only ~2 cm^{-1}, which means that the inclusion of the bending motion affects the fundamental frequency of Be-O stretching motion only marginally. This leads us to neglect the bending motion in the MC simulations, since it is highly expensive to construct the XeBeO-Rg potential energy surface when all vibrational modes of XeBeO are included. The fundamental frequency for ArBeO is blueshifted by 80 cm^{-1} from BeO in 2D-DVR calculations, and it is slightly larger than that of XeBeO, which is consistent with the previous work.[7] This shift is relatively close to the experimental value of 62 cm^{-1}, which was measured in Ar matrix (see Table I), and it may be predicted that the effect of surrounding Ar atoms is small. The bond length of Be-O is again almost unchanged upon formation of ArBeO. From the same reason as above, the MC simulations for ArBeO-Ar_N are performed using 2D-DVR for solving the vibrational energy levels of ArBeO.

B. Potential energy surfaces for XeBeO-Xe, XeBeO-Ar, and ArBeO-Ar

Figure 3 shows the two-dimensional contour plots of the potential energy surfaces for XeBeO-Xe, XeBeO-Ar, and ArBeO-Ar, where the internal coordinates of XeBeO and ArBeO are fixed at the equilibrium values. As can be seen in the figure, three local minima were located for each potential, where two of them are on both side of the molecule in collinear geometry. The binding energies of Xe to XeBeO for these collinear configurations are 0.906 and 1.893 kcal/mol on the Xe (Structure-I) and O sides (Structure-II), respectively. Another minimum is located between and almost equidistant from Be and O atoms with a binding energy of 1.653 kcal/mol (Structure-III). The binding energies of Ar to XeBeO and ArBeO for these three minima are tabulated in Table III. These

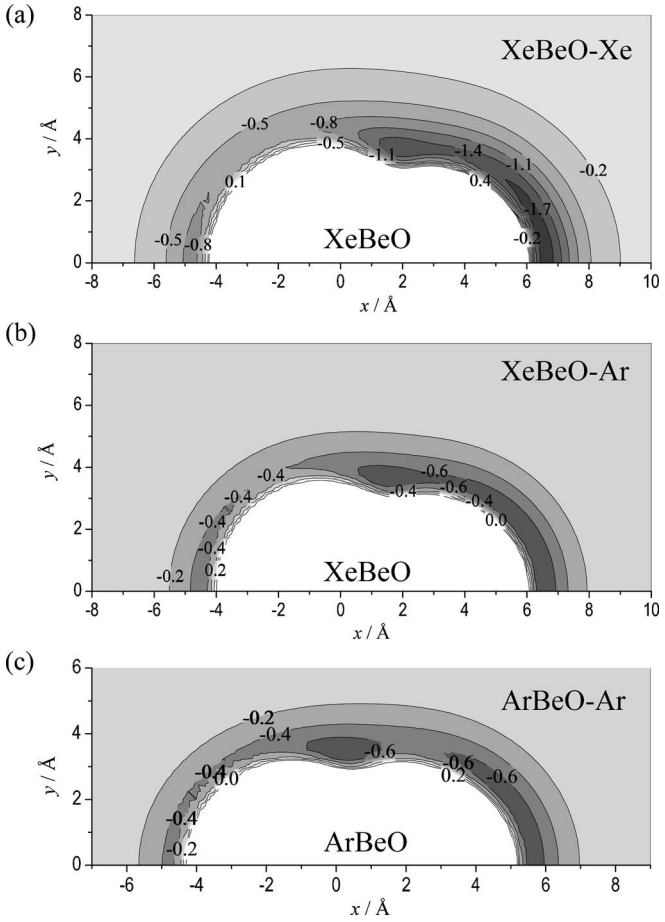

FIG. 3. Two-dimensional contour plots of the potential energy surfaces (in units of kcal/mol) for (a) XeBeO-Xe, (b) XeBeO-Ar, and (c) ArBeO-Ar. The internal coordinates of RgBeO (Rg = Xe or Ar) are fixed at the equilibrium values and the origin is set to the center-of-mass of RgBeO. The positions of the Xe, Be, and O are (−0.51, 0.0), (1.84, 0.0), and (3.17, 0.0), respectively, for XeBeO, and those of the Ar, Be, and O atoms are (−1.12, 0.0), (0.94, 0.0), and (2.27, 0.0), respectively, for ArBeO.

values at three local minima for XeBeO-Xe (XeBeO-Ar or ArBeO-Ar) are almost in the same order as in the Xe-Xe (Ar-Ar) interaction.

The validity of the pairwise-additive description of the potential energy for RgBeO-Rg$_N$ system, as is given in Eq. (2.1), should of course be examined. For this purpose, the interaction energy of XeBeO-Xe$_6$ cluster is compared between the *ab initio* method and pairwise-additive model. We randomly choose several configurations from the MC simulations of XeBeO-Xe$_{500}$ cluster (which will be detailed later) and the nearest six Xe atoms to XeBeO are taken to form XeBeO-Xe$_6$ clusters. As a result of comparison, differences between the interaction energies by the *ab initio* method and the pairwise-additive model were calculated to be ∼0.1 kcal/mol for all cases, which shows a good agreement with each other. More importantly, the fundamental frequencies were compared between these two potentials and the differences were only ∼0.2 cm^{-1} for 2D-DVR calculations, which gives confidence in the reliability of the pairwise-additive model for RgBeO-Rg$_N$ systems.

TABLE III. Binding energies (in kcal/mol) of Xe or Ar to RgBeO.

	XeBeO-Xe	XeBeO-Ar	ArBeO-Ar
Structure-I	0.906	0.481	0.449
Structure-II	1.893	0.761	0.715
Structure-III	1.653	0.752	0.787

C. Monte Carlo simulations for XeBeO-Xe$_N$, XeBeO-Ar$_N$, and ArBeO-Ar$_N$

The MC simulations were performed for XeBeO in solid Xe and Ar and for ArBeO in solid Ar under the periodic boundary condition (PBC) at temperature of $T = 30$ K. The fcc lattice was taken as a starting point for the initial configuration and 500 Xe (500 Ar) atoms were placed in a cubic box with a cell length of 30.6 Å (26.6 Å), which yields a density of 3.78 g/cm^3 (1.76 g/cm^3) and is close to the experimental value at the saturated vapor condition.[18] There are several possible sites at which Rg atom(s) can be substituted by RgBeO. As shown in Figure 4, one or two Rg atoms along the three possible orientations were replaced with a single RgBeO and these configurations were used to initiate MC simulations. The number of substituted Rg atoms was determined from a sensible choice based on the distance between the adjacent atoms along each orientation and it is shown in Table IV. After equilibrating the system, a total of 10^6 MC steps were taken to obtain statistical averages. Here, in each MC step, 100 steps were used on the approximate potential that is given in Eq. (2.5).

The MC results are summarized in Table IV, where the peak positions of Be-O vibrational spectra of RgBeO are given, along with the full width at half maximum (FWHM) values of the vibrational spectra. We also evaluate the interaction energies between RgBeO and other surrounding Rg atoms in order to compare the stability of each site. The

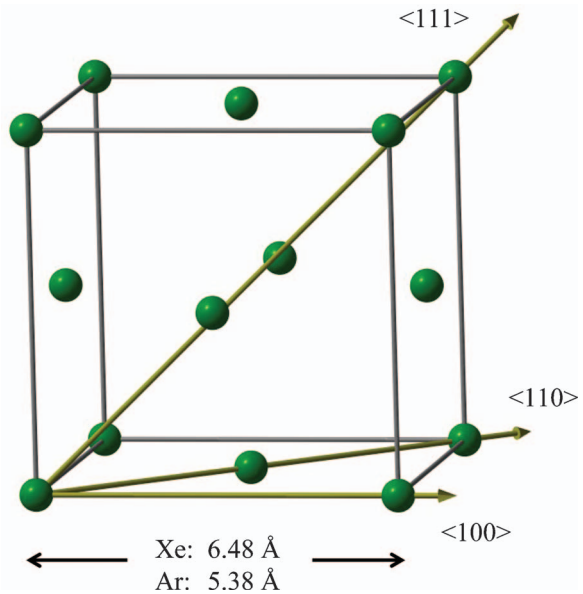

FIG. 4. Fcc lattice structure of solid Xe or Ar. The three possible orientations of RgBeO are depicted as ⟨100⟩ (four-atomic window), ⟨110⟩ (nearest neighbor), and ⟨111⟩ (three-atomic window).

TABLE IV. Peak positions of vibrational spectra (in cm^{-1}) of Be-O stretching motion of RgBeO and interaction energy (in kcal/mol) in solid Xe and Ar under PBC. The FWHM values (in cm^{-1}) of the vibrational spectra are also shown. N_r is the number of rare gas atom(s) replaced with a single RgBeO. The shifts from the gas phase values (1537 cm^{-1} for XeBeO and 1539 cm^{-1} for ArBeO) are shown in the last column.

	N_r	Frequency	FWHM	V_{int}	Shift
		XeBeO in solid Xe			
⟨100⟩	1	1543	8	−18.7	+6
⟨110⟩	2	1516	3	−20.0	−21
⟨111⟩	1	1513	7	−19.2	−24
		XeBeO in solid Ar			
⟨100⟩	1	1544	7	−11.0	+7
⟨110⟩	2	1529	3	−13.1	−8
⟨111⟩	1	1538	7	−11.2	+1
		ArBeO in solid Ar			
⟨100⟩	1	1560	7	−9.6	+21
⟨110⟩	2	1531	3	−12.4	−8
⟨111⟩	1	(1531)	(3)	(−12.4)	(−8)

interaction energy is simply defined as

$$\langle V_{int}\rangle = \left\langle E^0_{qm}(\mathbf{R})\right\rangle - E^0, \tag{3.1}$$

where $E^0_{qm}(\mathbf{R})$ is the vibrational ground state energy of RgBeO that includes the interaction with surrounding Rg atoms, which is given in Eq. (2.4), and E^0 is that in the gas phase. The Rg atoms whose distances from the center-of-mass of RgBeO are within the half of the length of the unit cell are taken into account to calculate the above interaction energies. In an ideal simulation, one could discuss the stability of each site by exploring all possible configurations in a long MC run, but at this low temperature, once RgBeO is inserted in one site, it is practically impossible to observe the migration between the sites within a routinely used number of MC steps. By using more sophisticated approaches such as the multicanonical algorithms, it may be possible to compare the stability of each site directly, but in this paper we simply use the interaction energy as a measure of the stability.

In the simulations of XeBeO in solid Xe, the different spectral shifts were observed depending on the substituted sites, as shown in Table IV. When comparing the interaction energies, the ⟨110⟩ site exhibits the lowest one, and this configuration would be most likely observed. Of course, we cannot exclude the possibility that the ⟨111⟩ site is observed since the difference in the interaction energy is only 0.8 kcal/mol. The redshifts from the gas phase value of XeBeO were observed for the ⟨110⟩ and ⟨111⟩ sites, while the blueshift was seen for the ⟨100⟩ site. Figure 5 shows the contour plots of two-dimensional distribution function of the Xe atoms around XeBeO, where the x axis is taken as the molecular axis of XeBeO and r is the radial distance from the x axis. Here the origin is set to the center-of-mass of XeBeO. As seen in the figure, the positions of the Xe atoms are quite localized. Apparently wider distribution in the ⟨110⟩ site compared to the other two sites is attributed to the larger fluctuations of the molecular axis of XeBeO in the ⟨110⟩ site. When comparing the peak positions of the Xe atoms, a significant difference between the sites is the locations of the Xe atoms in the collinear geometry. In the ⟨100⟩ site, one Xe atom is positioned on the O side at $x \approx 6.5$ Å, while it is $x \approx 8.0$ Å and 9.5 Å for the ⟨110⟩ and ⟨111⟩ site, respectively. As seen in the potential energy surface of XeBeO-Xe given in Figure 3(a), this Xe atom in the ⟨100⟩ site is slightly pushed toward the O atom from the minimum of the potential energy surface and is close to the repulsive region. This makes the potential energy surface of XeBeO for solving the vibrational energy levels slightly narrower, especially along the Be-O vibration coordinate (q_1), resulting in the blueshift in the spectra. The observed redshifts in the ⟨110⟩ and ⟨111⟩ sites would be simply attributed to the attractive interactions between XeBeO and surrounding Xe atoms. Similar observations were seen in the simulations of XeBeO and ArBeO in solid Ar, where the ⟨110⟩ sites exhibit the lowest interaction energies. In the simulation of ArBeO in solid Ar, it is seen that an MC run starting from the ⟨111⟩ site resulted in the same configuration as the ⟨110⟩ site after equilibration. In both simulations, the redshifts from the gas phase values of RgBeO were observed in the ⟨110⟩ site, while the blueshifts were seen in the ⟨100⟩ site. The observed blueshift is also due to the mild packing of neighboring Ar atoms along the ⟨100⟩ direction, and the redshift is owing to the attractive interactions.

In order to investigate in more detail how the Rg atoms are distributed around RgBeO during the crystallization, we performed MC simulations for XeBeO-Xe_N, XeBeO-Ar_N, and ArBeO-Ar_N clusters with $N = 500$. A total of ten independent simulations were performed at $T = 30$ K. Prior to each simulation, the system was heated up to 150 K under the confinement potential and after a sufficient number of steps at 150 K where the cluster exhibited liquid-like behavior, it was cooled down to 30 K gradually with a decrement of 10 K. The confinement potential has a functional form of $V = (r/R_{conf})^{20}$, where r is the distance of Rg from the center-of-mass of the cluster and R_{conf} is a parameter to determine the size of the confinement potential. Note that this confinement potential is added to prevent the evaporation of Rg atoms at 150 K and is removed at 30 K. At this low temperature of 30 K, once the atomic configurations are determined, the atoms do not change their positions frequently because the clusters are in the solid phase. As expected, the clusters exhibit a somewhat amorphous-like structure, and the configurations of the Rg atoms around RgBeO were different in each simulation due to the technical difficulty of crystallization in MC simulations, also because the existence of the impurity made it more difficult to form the crystal structure around it. Since there are a huge number of stable structures even for clusters with small number of Rg atoms, each MC run is trapped in one of these configurations. Thus, the peak positions of vibrational spectra from different MC runs scattered to some extent, but it was observed that they were within a relatively narrow range, except for two MC runs in the XeBeO-Xe_N clusters.

In Table V, the average values of peak positions of vibrational spectra and their standard deviations from ten MC runs are shown. As seen in the table, the standard deviations are small for all three types of clusters. In the simulations of XeBeO-Xe_N clusters, the above-mentioned two MC runs are excluded when calculating the averages. These two runs

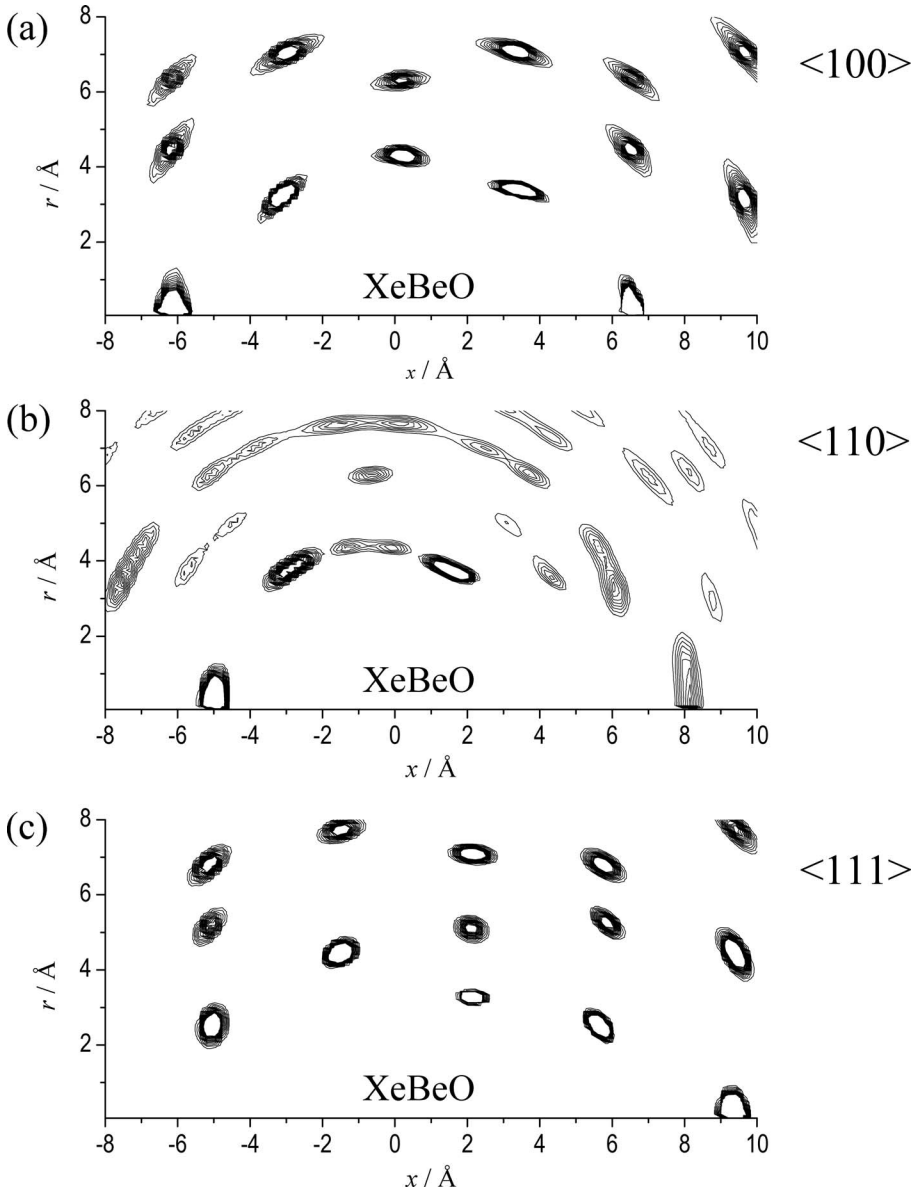

FIG. 5. Contour plots of two-dimensional distribution functions of the Xe atoms around XeBeO for the (a) ⟨100⟩, (b) ⟨110⟩, and (c) ⟨111⟩ sites. The positions of XeBeO are the same as those in Figure 3.

have peak frequencies of 1544 and 1542 cm^{-1} and interaction energies of −19.0 and −18.9 kcal/mol, and these values are close to the ones at the ⟨100⟩ site. When inspecting the two-dimensional distribution functions for these two runs, it was found that the Xe atom was located around $x = 6.5$ Å in the collinear geometry, which is typical of the ⟨100⟩ site. For the other eight runs, the vibrational frequencies and interaction energies are close to the ones at the ⟨110⟩ and ⟨111⟩ sites. When we examine the configurations of the Xe atoms around XeBeO, however, it was difficult to distinguish which sites were formed inside the cluster since in some cases the Xe atoms were not found in collinear geometry of XeBeO as was observed in the simulations of solid Xe. Judging by the distribution functions, some runs could be assigned to the ⟨110⟩ site, but in some other runs, they were found to be more like the ⟨111⟩ site. On the other hand, in the simulations of XeBeO-Ar_N and ArBeO-Ar_N clusters, the average values of frequency and interaction energy are in good agreement with those at the ⟨110⟩ site and the distribution functions of each simulation bear a close resemblance to those of the ⟨110⟩ site. It is safe to say that the ⟨110⟩ site is most likely formed for these clusters. In all three types of clusters, at least it was confirmed that the redshifts were observed, and the interaction energies are close to those at the ⟨110⟩ site. From the above

TABLE V. The average values of peak positions of vibrational spectra (in cm^{-1}) and interaction energies (in kcal/mol) from ten independent MC simulations. The standard deviations are shown in parenthesis.

	Frequency	V_{int}
XeBeO-Xe_N	1513 (1.9)	−20.6 (0.31)
XeBeO-Ar_N	1530 (1.6)	−13.2 (0.15)
ArBeO-Ar_N	1532 (1.3)	−12.5 (0.23)

TABLE VI. Summary of the present work and experimental data on vibrational frequency (in cm^{-1}). The frequencies shown as solid Xe and Ar are taken from the ⟨110⟩ site. The vibrational shifts from the gas phase values of BeO are included in parenthesis.

	BeO	XeBeO	XeBeO in solid Xe	XeBeO in Xe cluster
This work	1459	1537 (+78)	1516 (+57)	1513 (+54)
Expt.	1464	...	1498 (+34)	
			XeBeO in solid Ar	XeBeO in Ar cluster
This work			1529 (+70)	1530 (+71)
Expt.			1517 (+53)	
		ArBeO	ArBeO in solid Ar	ArBeO in Ar cluster
This work		1539 (+80)	1531 (+72)	1532 (+73)
Expt.		...	1526 (+62)	

simulations on clusters and also those under PBC, it would be naturally expected that the ⟨110⟩ site would represent a plausible configuration inside the matrices.

In summary, the vibrational shift from the isolated BeO was calculated to be 57, 70, and 72 cm^{-1} for XeBeO in solid Xe, XeBeO in solid Ar, and ArBeO in solid Ar, respectively, at the ⟨110⟩ site, and 54, 71, and 73 cm^{-1} from the calculations of clusters (see Table VI). These values are in reasonable agreement with experimental data of 34, 53, and 62 cm^{-1}. We note, however, that these shifts depend strongly on the quality of the potential and it would improve the agreement by performing more accurate *ab initio* calculations. Of course, there is also room for improvement in the methodology. As shown in the gas phase calculation of RgBeO, the inclusion of Rg-Be-O bending motion slightly lower the vibrational frequency, therefore if we perform 3D-DVR MC simulation, it would predict more closer value to the experimental one. However, given the quality of the interaction potential employed in this study, we believe that it successfully reproduces the experimental observations.

IV. CONCLUSION

In this study we performed mixed quantum-classical simulations for vibrational spectra of BeO in the Xe and Ar matrix environments and investigated the origin of spectral shift in detail. The high-level *ab initio* calculations were carried out to determine the interaction potential needed to construct the total potential of the system, and the MC simulations were performed using this potential in order to obtain vibrational spectra in the presence of surrounding rare gas atoms.

It was found that the BeO molecule forms stable XeBeO or ArBeO complex inside the rare gas matrices, which alone induces the blueshift in the vibrational spectra of 78 cm^{-1} and 80 cm^{-1}. When the effect of other surrounding rare gas atoms is included, the vibrational frequency is redshifted from that of XeBeO complex by 21 cm^{-1} in solid Xe and 8 cm^{-1} for ArBeO in solid Ar. The calculated shifts were in reasonable agreement with experimental results.

In conclusion, it is already known that the spectral shift due to the formation of RgBeO complex is not negligible, but the vibrational shift originating from the other surrounding rare gas atoms should be carefully taken into account for quantitative description of the spectral shifts, and therefore the observed shifts are the outcome of the competing effects of rare gas atoms in matrix environments. We are now investigating these effects on other molecules and examine whether this finding also applies to other systems. Also, we are interested in vibrational spectroscopy of exotic molecule HXeCl or HXeBr,[19–21] where pronounced complexation effects are observed due to the relatively weak bonding and large dipole moments.[22] The peculiar matrix shift of H-Xe stretching motion in HXeCl, which was observed in neon,[19] kryption,[20] and xenon[20] matrices, is still not well understood, and we are currently working to scrutinize the origin of the matrix shift in these systems.

ACKNOWLEDGMENTS

The authors acknowledge the financial support by a Grant-in-Aid for Challenging Exploratory Research from the Ministry of Education, Culture, Sports, Science and Technology (MEXT, Japan). Part of the calculations was performed on supercomputers at Research Center for Computational Science, Okazaki, Japan.

[1] M. F. Zhou, L. Andrews, and C. W. Bauschlicher, Chem. Rev. **101**, 1931 (2001).
[2] C. J. Evans and M. C. L. Gerry, J. Chem. Phys. **112**, 9363 (2000).
[3] Y. Y. Zhao, Y. Gong, and M. F. Zhou, J. Phys. Chem. A **110**, 10777 (2006).
[4] Y. Taketsugu, T. Noro, and T. Taketsugu, J. Phys. Chem. A **112**, 1018 (2008).
[5] G. Frenking, W. Koch, J. Gauss, and D. Cremer, J. Am. Chem. Soc. **110**, 8007 (1988).
[6] C. A. Thompson and L. Andrews, J. Am. Chem. Soc. **116**, 423 (1994).
[7] A. Veldkamp and G. Frenking, Chem. Phys. Lett. **226**, 11 (1994).
[8] C. A. Thompson and L. Andrews, J. Chem. Phys. **100**, 8689 (1994).
[9] K. P. Huber and G. Herzberg, *Constants of Diatomic Molecules*. (Van Nostrand Reinhold, New York, 1979).
[10] G. Igelmann, H. Stoll, and H. Preuss, Mol. Phys. **65**, 1321 (1988).
[11] R. P. White, S. M. Cleary, and H. R. Mayne, J. Chem. Phys. **123**, 094505 (2005).
[12] H.-J. Werner, P. J. Knowles, R. Lindh, F. R. Manby, M. Schütz *et al.*, MOLPRO, version 2008.1, a package of *ab initio* programs, 2008, see http://www.molpro.net.
[13] J. C. Light, I. P. Hamilton, and J. V. Lill, J. Chem. Phys. **82**, 1400 (1985).
[14] J. Echave and D. C. Clary, Chem. Phys. Lett. **190**, 225 (1992).
[15] D. T. Colbert and W. H. Miller, J. Chem. Phys. **96**, 1982 (1992).
[16] L. D. Gelb, J. Chem. Phys. **118**, 7747 (2003).
[17] A. Nakayama, N. Seki, and T. Taketsugu, J. Chem. Phys. **130**, 024107 (2009).
[18] G. L. Pollack, Rev. Mod. Phys. **36**, 748 (1964).
[19] M. Lorenz, M. Räsänen, and V. E. Bondybey, J. Phys. Chem. A **104**, 3770 (2000).
[20] M. Pettersson, J. Lundell, and M. Räsänen, J. Chem. Phys. **102**, 6423 (1995).
[21] Z. Bihary, G. M. Chaban, and R. B. Gerber, J. Chem. Phys. **116**, 5521 (2002).
[22] L. Khriachtchev, M. Räsänen, and R. B. Gerber, Acc. Chem. Res. **42**, 183 (2009).